1521-0111/12/8201-80–89$25.00
MOLECULAR PHARMACOLOGY
Copyright © 2012 The American Society for Pharmacology and Experimental Therapeutics
Mol Pharmacol 82:80–89, 2012

Vol. 82, No. 1
77818/3777073

Effects of Nucleotide Analogs at the P2X3 Receptor and Its Mutants Identify the Agonist Binding Pouch[S]

Thomas Riedel, Sara Wiese, Anna Leichsenring, and Peter Illes

Rudolf Boehm Institute for Pharmacology and Toxicology, University of Leipzig, Leipzig, Germany

Received January 16, 2012; accepted April 11, 2012

ABSTRACT

In this study, we investigated the effects of single alanine substitutions of amino acid residues in the supposed ATP binding site of the human P2X3 receptor on the agonistic effect of nucleotide analogs. The wild-type and mutant receptors were expressed in HEK293 cells, and the nucleotide effects were measured by means of the whole-cell patch-clamp method. Modifications in the receptor binding site changed the concentration-response relationship, the current kinetics, and the recovery from desensitization during fast, pulsed, local agonist applications. On the basis of this fact, we were able to distinguish binding from other effects, such as gating/desensitization, by using a hidden Markov model that describes the complete channel behavior with a matrix of rate constants. The binding energies of the nucleotide analogs were calculated and compared with the binding energies of ATP at both the wild-type receptor and its alanine mutants. Changes in the binding energies caused by alterations in the receptor and/or agonist structures were concluded to be attributable to the preferential binding of certain structural constituents of ATP to certain amino acid moieties of the receptor. The results were also checked for consistency with a P2X3 homology model that we developed from the known zebrafish P2X4 crystal structure in the closed state. The functional data correlated well with the predictions of the agonist dockings to the structural model.

Introduction

P2X receptors are ATP-gated cation channels with seven subtypes (P2X1–7) (Khakh et al., 2001; North, 2002; Köles et al., 2007). Despite the structural similarity between P2X receptors and acid-sensing ion channels (ASICs) (i.e., two transmembrane domains, extracellular loop, and intracellular N- and C-terminal tails), these two receptor families do not share amino acid (AA) similarity (Gonzales et al., 2009). For many years, knowledge of the AA residues possibly involved in agonist and antagonist binding, allosteric modulation, desensitization, and channel-gating was derived from mutagenesis studies (Khakh et al., 2001; North, 2002; Egan et al., 2004; Roberts et al., 2006). Many AAs in the extracellular loop were mutated for this purpose, and it was concluded that especially conserved AAs organized in four clusters [termed, for example, nucleotide-binding segments (NBS) by Mager et al., 2004] are important for ATP binding (Jiang et al., 2000; Roberts and Evans, 2007; Zemkova et al., 2007).

Overwhelming evidence indicates that three homologous or heterologous subunits combine to form a trimeric P2X receptor (Nicke et al., 1998; Aschrafi et al., 2004; Young et al., 2008; Shinozaki et al., 2009). The original model assumed that each P2X subunit contains one individual binding site for ATP (Vial et al., 2004), but it soon became clear that binding probably occurs at the interface between two neighboring subunits (Wilkinson et al., 2006; Marquez-Klaka et al., 2009). Earlier electrophysiological studies (Bean, 1990; Ding and Sachs, 1999) and molecular simulation of the agonist-induced currents (Sokolova et al., 2006; Karoly et al., 2008) both suggested that at least two agonist molecules are necessary for receptor activation. The published crystal structure of the zebrafish (zf) P2X4 receptor at a resolution of 3.1 Å fully confirmed both the trimeric architecture of the P2X receptor family and the location of the agonist binding pouch between two subunits in the extracellular domain (Kawate et al., 2009; Browne et al., 2010; Young, 2010). The AA residues that were suggested to be essential for agonist binding in mutagenesis studies were found to be oriented toward the groove of the pouch, which indicates that they may bind an ATP molecule.

This work was supported by the Deutsche Forschungsgemeinschaft (Research Unit FOR748) [Grants RI 2092/1-2, IL 20/18-2].

T.R. and S.W. contributed equally to this work.

Article, publication date, and citation information can be found at http://molpharm.aspetjournals.org.
http://dx.doi.org/10.1124/mol.112.077818.

[S] The online version of this article (available at http://molpharm.aspetjournals.org) contains supplemental material.

ABBREVIATIONS: ASIC, acid-sensing ion channel; AA, amino acid; NBS, nucleotide-binding segment; R.M.S.D., root mean square deviation; wt, wild-type; zf, zebrafish; me-ATP, methylene-ATP; ATP-γ-S, adenosine 5′-*O*-(γ-thio)triphosphate; 2-MeS-ATP, 2-methylthio-ATP; TNP-ATP, trinitrophenyl-ATP; Bz-ATP, dibenzoyl-ATP.

Despite this direct and indirect evidence, the exact position of ATP within the binding pocket of P2X receptors and the structural prerequisites for the physical interactions between ATP and the individual AA residues relevant for its binding remain largely unknown. The aim of our study was to acquire knowledge about the agonist binding sites of the pain-relevant P2X3 receptor. Starting from the key-lock view of receptor-ligand binding, we modified both the ligand (key), by using structural analogs of ATP as agonists, and the binding pocket at the receptor (lock), by using Ala mutants of the P2X3 receptor, to determine which keys fit the changed lock. The strategy of double-mutant cycles (Horovitz, 1996) was used to analyze the interactions between agonists and AAs within the binding pouch. We suggest a binding configuration for ATP in which the adenine is located deep in the binding pocket and Lys65, as a central AA, coordinates the purine, the ribose, and the β-phosphate; the γ-phosphate appears to be bound to Arg281.

Materials and Methods

Cell Culture and Mutagenesis. HEK293 cells were kept at 37°C, in humidified air (with 10% CO_2), in Dulbecco's modified Eagle's medium (Sigma-Aldrich, St. Louis, MO) with 4.5 mg/ml D-glucose, 1% L-glutamine, and 10% fetal bovine serum. The human P2X3 receptor cDNA was subcloned into pIRES2-EGFP vector (Clontech Laboratories, Mountain View, CA) by using PstI and EcoRI restriction sites. All P2X3 receptor mutants were generated by introducing replacement mutations with the QuikChange site-directed mutagenesis protocol (Agilent Technologies, Santa Clara, CA). Individual AA residues located in one of the four nucleotide-binding segments (Mager et al., 2004) of the P2X3 receptor were replaced with Ala (Bodnar et al., 2011). Before transfection, the cells were plated in plastic dishes. For each dish, 0.5 μg of plasmid cDNA for the receptor mutants, 100 μl of OptiMEM, and 10 μl of PolyFect transfection reagent (QIAGEN, Valencia, CA) were mixed for 10 min and then added to the cells. To remove residual plasmid cDNA, the medium was replaced with OptiMEM after 18 h of incubation.

Electrophysiological Studies. Whole-cell patch-clamp recordings were performed 2 to 3 days after transient transfection of the HEK293 cells, at room temperature (20–22°C), by using an Axopatch 200B patch-clamp amplifier (Molecular Devices, Sunnyvale, CA). The pipette solution contained 135 mM CsCl, 1 mM $CaCl_2$, 2 mM $MgCl_2$, 20 mM HEPES, 11 mM EGTA, and 0.3 mM guanosine 5′-*O*-(γ-thio)triphosphate (Sigma-Aldrich); the pH was adjusted to 7.3 with CsOH. The external physiological solution contained 5 mM KCl, 135 mM NaCl, 2 mM $MgCl_2$, 2 mM $CaCl_2$, 10 mM HEPES, and 11 mM glucose; the pH was adjusted to 7.4 with NaOH. The pipette resistances were 3 to 7 MΩ, the membrane resistance was 0.1 to 2 GΩ, and the access resistances were 3 to 12 MΩ. All recordings were performed at a holding potential of −65 mV. Data were filtered at 2 kHz with the inbuilt filter of the amplifier, digitized at 5 kHz, and recorded by using a Digidata 1440 interface and pClamp10.2 software (Molecular Devices).

Drugs were dissolved in external solution and were superfused to single cells by using a rapid solution-exchange system (SF-77B Perfusion Fast Step; Warner Instruments, Hamden, CT). To estimate the solution-exchange times of the system, KCl (150 mM) was applied to the cell and the resulting current was recorded. The time constant of solution exchange was determined with a single exponential fit, to adjust the wash-in and wash-out of the drugs. Between drug applications, the cells were continuously superfused with the standard external solution.

First, HEK293 cells transfected with the wild-type (wt) P2X3 receptor were used to determine the effects of ATP and its analogs. Concentration-response curves were generated by applying increasing concentrations (up to 300 μM) of ATP and its derivatives for 2 s each. The structural analogs of ATP used exhibited modifications either in the nucleoside core or in the attached phosphate groups (Fig. 1). They were as follows: dATP, CTP, GTP, α,β-methylene-ATP (α,β-me-ATP), β,γ-methylene-ATP (β,γ-me-ATP), adenosine 5′-*O*-(γ-thio)triphosphate (ATP-γ-S) (all from Sigma-Aldrich), and 2-methylthio-ATP (2-MeS-ATP) (Tocris Bioscience, Ellisville, MO). In agreement with previous results (Gerevich et al., 2007), a 5-min period was required to allow P2X3 receptors to recover from desensitization. Because of the long recovery time for 2-MeS-ATP at the wt receptor (Sokolova et al., 2004), the interapplication interval was prolonged to 10 min for this agonist.

HEK293 cells were transiently transfected with mutant cDNA for the following nucleotide binding sites: NBS1 (K63A and K65A), NBS2 (F174A and K176A), NBS3 (N279A and R281A), and NBS4 (L297A, K299A, and F301A). We then constructed concentration-response curves for a number of ATP structural analogs (see above). Moreover, recovery protocols for all mutant-substance combinations were produced by applying a high agonist concentration for 2 s, again after a 2-s interval, and finally after an additional 60-s interval.

Kinetic Fit of P2X3 Current with Hidden Markov Model. The Markov model for P2X3 used in this study (Fig. 2C) (for detailed description, see *Results*) was based on proven models (Sokolova et al., 2006; Karoly et al., 2008). The fixed factors that ensure microscopic reversibility were replaced by the more-flexible loop-balance function provided by QuB software (http://www.qub.buffalo.edu) (Milescu et al., 2005). Because there was no obvious reason to exclude direct transition between the two- and three-liganded open states, this transition was included. The binding and unbinding rates were constrained to the other binding steps of the closed channel. During the fitting process, the rates between the open and desensitized states were found to be close to 0. Therefore, we concluded that a direct transition was unlikely and we removed it from our calculations.

There are no available data on the open times of P2X3. Single-channel measurements of rat P2X3 receptors could not resolve the individual events with 1-kHz filtering and 5-kHz sampling rates (Evans, 1996; Grote et al., 2005). We assumed that the open times of human P2X3 receptors were of the same magnitude as those from

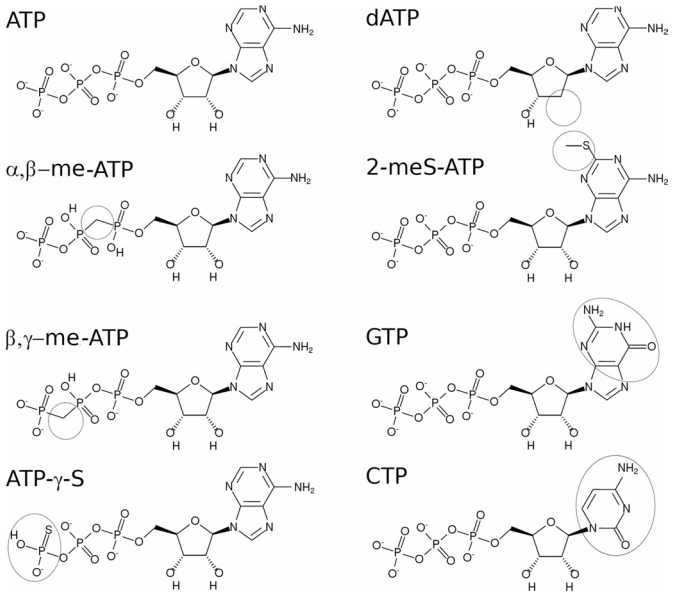

Fig. 1. Chemical structures of ATP, its structural analogs, and CTP. The gray circles indicate the positions where a structural modification was performed. The protonation state for pH 7.4 was calculated with OpenBabel (see *Materials and Methods*). The benzoyl and trinitrophenyl residues of Bz-ATP and TNP-ATP were attached to the ribose moiety (not shown).

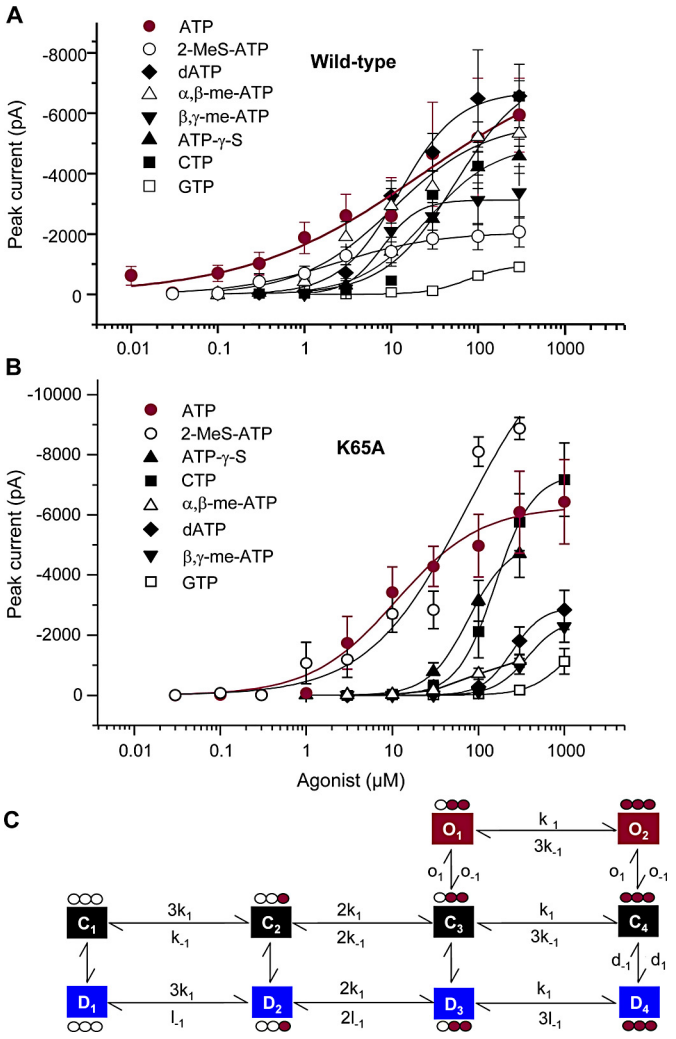

Fig. 2. Concentration-response curves for ATP, its structural analogs, and CTP with the wt P2X3 receptor and its K65A mutant expressed in HEK293 cells. The logarithmic agonist concentration was plotted against the peak current amplitude. A, concentration-response curves for the wt P2X3 receptor. B, concentration-response curves for the K65A mutant of the P2X3 receptor. Values are mean ± S.E.M. of four to 16 experiments in A and B. C, kinetic model with two open states for simulation of the concentration-response curves and analysis of the binding, gating, and desensitization processes. The forward (k_1) and backward (k_{-1} and l_{-1}) rate constants characterizing transitions between the unbound, closed-state receptor (C_1) and the receptor binding one (C_2), two (C_3), or three (C_4) agonist molecules, as well the two open-state receptors (O_1 and O_2) and the desensitized receptors (D_1, D_2, D_3, and D_4), are indicated. The forward (d_1) and backward (d_{-1}) rate constants characterizing transitions between C_4 and D_4 are also shown. The filled circles represent the occupied agonist binding sites of the three possible ones.

rats. Therefore, the rate of transition from open to closed states should be at least 1000 events per s. We fixed the closing rate to 1000 events per s to maintain the supposed open time of approximately 1 ms. During the fit of wt P2X3 currents, the opening rate increased up to the limit set at 10,000 events per s. The determination of this rate was vague, but the influence on macroscopic currents was marginal. For additional analyses, the opening rate was fixed to this value.

The rates that described the recovery from desensitization were slow and had no significant effect within the 2-s agonist application periods used for the construction of concentration-response curves. To determine these rates, the effects of three pulses delivered with 2- and 60-s intervals were analyzed.

The number of channels in the membrane of a single cell and the proportions of those channels in open or desensitized states are unknown. These two parameters have a strong influence on each other, because a channel that transitioned directly to the desensitized state would not be recognized in our measurements. Furthermore, the absolute numbers of channels differ from cell to cell, and the channel number must be a free parameter.

The resulting model, which was validated for ATP action at wt P2X3 receptors, includes a relatively low number of free parameters (only 11) that describe the entire kinetic pattern of P2X3 over a wide range of agonist concentrations. This initial model was further constrained to preserve the relationships between the desensitization rates. The final model used for agonist- and mutant-dependent fits had only four independent parameters, namely, agonist binding (k_1) and dissociation (k_{-1}), desensitization (d_1), and recovery (d_{-1}) (Fig. 2C). The number of ion channels per cell was taken as an additional free parameter; l_{-1} depended on the residual rate constants attributable to the constraints of the model.

Because P2X3 channels open very quickly, especially at high agonist concentrations, the measured current kinetics are influenced by the speed of solution exchange. The fast simultaneous opening of channels led to distortion of the recorded signals, because of the limitation of the maximal measurable current by the access resistance, R_a. To avoid these complicating factors, we analyzed smaller and slowly activating currents induced by low agonist concentrations. We included corrections in our model by describing the wash-in and wash-out phases with an exponential function instead of a simple rectangular pulse. The time constant of solution exchange (τ = 140 ms) was determined through application of a 150 mM potassium test pulse. Conductance of the channels was calculated with the following formula, which compensates for the influence of R_a and R_m: $\sigma = (R_a + R_m)^2/[R_a^2 R_m + R_a R_m^2 + (R_m^2 U_h/I)]$, where I is the measured current, U_h the holding potential, R_a the access resistance, and R_m the membrane resistance. The number of receptor channels may vary from cell to cell; therefore, this was determined to be a free parameter.

Comparison of Binding Energies. The dissociation constant K_D and the binding energy ΔG for a mutant-agonist combination were calculated from the fit parameters k_1 and k_{-1} from the Markov model with the equations $K_D = k_{-1}/k_1$ and $\Delta G = RT\ln K_D$, where R is the gas constant and T is absolute temperature.

All tested alanine substitutions were in the supposed binding pocket (Bodnar et al., 2011) and led to reduced binding energies, compared with the wild-type receptor. The different agonists used differed also in their binding energies for the receptor. If the effects of the mutation and the modification of the agonist structure were independent, then the binding energy of this combination could be predicted from the binding energies of the separate experiments. The difference between the predicted and measured binding energies of a mutant-ligand combination is given by the following equation: $\Delta\Delta G = \Delta G^{\text{agonistX}}_{\text{mutant}} - [\Delta G^{\text{ATP}}_{\text{wt}} - (\Delta G^{\text{ATP}}_{\text{wt}} - \Delta G^{\text{ATP}}_{\text{mutant}}) - (\Delta G^{\text{ATP}}_{\text{wt}} - \Delta G^{\text{agonistX}}_{\text{wt}})]$. If the mutation and the agonist modification were in close spatial relationship in the binding pocket, then they would interact with each other. In that case, the predicted binding energy should differ from the measured value. Comparison of the predicted binding energies with the measured values provided information on how the agonists allocated to the protein. Because all mutated AAs were located within the binding pocket, we also expected nonspecific coupling between the mutations and ligand modifications. Therefore, we set an arbitrary energy threshold level of $\Delta\Delta G < 5$ kJ/mol, above which we assumed a specific direct interaction between the two modifications.

Homology Modeling of Human P2X3 Structure. We constructed our structural P2X3 receptor model from the published zfP2X4 crystal structure and the sequence of human P2X3 with the loopmodel function of the Modeler 9v8 program (http://salilab.org/modeller), by using a standard script with improved loop refinement (Fiser and Sali, 2003; Kawate et al., 2009). Visualization was performed with VMD (http://www.ks.uiuc.edu/Research/vmd), with the tachyon plugin (Humphrey et al., 1996).

Ligand Docking. Agonist structures were downloaded from the PubChem database (http://pubchem.ncbi.nlm.nih.gov). Protonation was adjusted for pH 7.4 with OpenBabel (http://openbabel.org/wiki/Main_Page), and structures were minimized through optimization with the MMFF94s force field. Flexible ligand docking to the homology model of the receptor was performed with AutoDock Vina (Trott and Olson, 2010), after preparation of the receptor and ligands with MGLTools 1.5.4 (http://mgltools.scripps.edu). The initial protein structure was minimized with NAMD (http://www.ks.uiuc.edu/Development/Download/download.cgi?PackageName=NAMD), in a water membrane system. After a global search with ATP in the whole binding cavity, a second analysis, with full flexible AA side chains and reduced search space, was performed for all ligands. The root mean square deviation (R.M.S.D.) values for the common atoms (PA, PB, PG, N1, C2, N3, C4, C5, C6, O1A, O2A, O1B, O2B, C1′, C2′, O3′, C3′, C4′, O5′, O4′, and C5′) were calculated with the RMSDTT 3.0 plugin of VMD.

Data Analysis. Concentration-response curves for all agonists were fitted by using a three-parameter Hill plot (OriginPro 8; OriginLab Corp., Northampton, MA). The I_{max} and EC_{50} values and the Hill coefficients are presented as mean ± S.E.M. of n experiments. One-way analysis of variance followed by the Holm-Sidak post hoc test was used for statistical analysis. A probability level of 0.05 or less was considered to reflect a statistically significant difference. Kinetic fits for the P2X3 current were calculated with QuB software; the binding energies of the mutant-agonist combinations were calculated from the fit parameters. The S.D. values for the binding energies were obtained from the propagated S.D. values for k_1 and k_{-1} in the kinetic fits.

Results

As shown in Fig. 2A, all agonists used induced concentration-dependent inward current responses at wt P2X3 receptors expressed in HEK293 cells. At lower concentrations, there was no or little desensitization; at higher concentrations, however, the effects rapidly decreased already during the 2-s agonist application time. The shapes of the currents were rather similar for the agonists, although ATP itself acted at lower concentrations, compared with its structural analogs, in causing comparable current amplitudes.

The concentration-response curves for CTP did not reach a clear maximum up to a concentration arbitrarily chosen as the upper limit (300 μM), and even the peak current with ATP reached only a relative maximum. Therefore, the I_{max} and EC_{50} values and Hill coefficients could not be calculated accurately for CTP and are only approximations for ATP (Fig. 2A). Otherwise, the comparison of the concentration-response curves for all agonists showed no statistically significant differences in potency (EC_{50} value), compared with that of ATP (Table 1). The I_{max} values for 2-MeS-ATP, dibenzoyl-ATP (Bz-ATP), and GTP differed from those of ATP, whereas the I_{max} values for the rest of the agonists did not. Bz-ATP kept the receptor desensitized for a very long time ($\tau_{recovery}$ = 638.5 ± 19.9 s; n = 3; data not shown) and produced a low maximal current with the present application protocol; its concentration-response curve was not included in Fig. 2A but the I_{max}, EC_{50}, and Hill coefficient are shown in Table 1. The Hill coefficient for ATP was near 1, which suggests that desensitization distorted the supposedly bimolecular or trimolecular interaction with the P2X3 receptor (Bean, 1990; Ding and Sachs, 1999). The slopes of the concentration-response curves for the structural analogs of ATP were rather variable (Fig. 2A). However, only the Hill coefficients for dATP and β,γ-me-ATP differed from that of ATP (Table 1); we have no explanation for this finding.

We excluded from our investigations the binding site mutants of P2X3 that did not respond to the prototypical agonist α,β-me-ATP (Bodnar et al., 2011) and to ATP up to 300 μM (K63A and K299A; data not shown), and we selected others that responded with smaller currents, compared with the wt receptor. The conserved AAs Lys65, Asn279, Arg281, and Leu297 were chosen, as well as the nonconserved AAs Phe174 and Phe301. It is interesting to note that, with the mutant K65A, there was a rightward shift of the concentration-response curve for ATP

TABLE 1

Maximal current responses (I_{max}) and half-maximal agonist concentrations (EC_{50}) of nucleotides at the wt P2X3 receptor and its K65A mutant expressed in HEK293 cells

Experimental concentration-response curves were determined with the whole-cell patch-clamp method. Simulated concentration-response curves were generated by means of a hidden Markov model (see *Materials and Methods* and Fig. 2C). A comparison of the experimental and simulated curves is shown in Supplemental Figure 1.

Receptor and Agonist	Experimental				Simulation	
	I_{max}	EC_{50}	Hill Coefficient	n	EC_{50}	Hill Coefficient
	pA	*μM*			*μM*	
wt						
ATP	5235 ± 1130	2.5 ± 1.8	0.85 ± 0.16	14	3.8 ± 0.1	0.91 ± 0.01
α,β-me-ATP	5218 ± 389	8.7 ± 2.7	1.26 ± 0.09	13	7.1 ± 0.2	0.96 ± 0.02
2-MeS-ATP	1831 ± 111*	1.5 ± 0.3	1.20 ± 0.08	7	0.74 ± 0.01	0.93 ± 0.01
dATP	6132 ± 762	10.5 ± 2.7	1.64 ± 0.18*	11	26.0 ± 0.9	0.97 ± 0.18
ATP-γ-S	4938 ± 371	26.0 ± 6.1	1.15 ± 0.15	5	13.7 ± 0.5	1.03 ± 0.03
β,γ-me-ATP	2828 ± 284	6.2 ± 0.9	3.77 ± 0.52*	7	29.1 ± 1.0	1.15 ± 0.01
Bz-ATP	608 ± 43*	2.6 ± 0.6	1.67 ± 0.44	4		
GTP	1467 ± 789*	171.8 ± 152.3	1.17 ± 0.16	8	243.7 ± 23.3	1.15 ± 0.04
CTP	8876 ± 5605	119.5 ± 177.5	1.18 ± 0.25	13	32.6 ± 1.2	1.03 ± 0.02
K65A						
ATP	6087 ± 1102	16.9 ± 8.0†	1.41 ± 0.16†	7	15.9 ± 0.4	1.01 ± 0.02
α,β-me-ATP	1332 ± 8*†	69.3 ± 0.8*†	1.71 ± 0.02*†	5	62.5 ± 3.2	1.08 ± 0.04
2-MeS-ATP	12,407 ± 4473	72.2 ± 83.0	0.76 ± 0.27	8	41.0 ± 1.3	1.12 ± 0.03
dATP	2934 ± 17*†	247.8 ± 2.2*†	2.47 ± 0.05*†	4	810.4 ± 8.3	1.70 ± 0.01
ATP-γ-S	5066 ± 106	76.6 ± 2.9*†	1.86 ± 0.09*†	4	442.3 ± 15.3	1.27 ± 0.02
β,γ-me-ATP	2533 ± 25*†	371.5 ± 5.5*†	2.27 ± 0.06*	4	2.1 ± 73.1	1.75 ± 0.01
CTP	7357 ± 15	157.7 ± 0.7*	1.99 ± 0.01*	4	597.5 ± 5.9	1.67 ± 0.01
GTP	2694 ± 68.2	1188.3 ± 45.5	1.92 ± 0.09	4	3299 ± 42.3	1.75 ± 0.01

* $P < 0.05$, statistically significant difference from the respective value with ATP as an agonist.
† $P < 0.05$, statistically significant difference from the respective value with the wt P2X3 receptor.

(higher EC_{50}), with no change in the I_{max}, compared with measurements with the wt receptor (Fig. 2, A and B; Table 1). In contrast, the maximum of the concentration-response curve for α,β-me-ATP was strongly depressed, and the EC_{50} value was much higher at the mutant receptor than at the wt receptor (Fig. 2, A and B; Table 1). In contrast to the wt P2X3, 2-MeS-ATP caused large but nonsaturating current responses at K65A, which prevented the accurate calculation of I_{max}, EC_{50}, and Hill coefficient values; GTP also failed to cause a maximal current up to 1000 μM (Fig. 2B; Table 1). We provide these values here to allow numeric comparison of the experimental and simulated data. The I_{max} and EC_{50} values for both β,γ-me-ATP and GTP at K65A differed from the corresponding values at the wt receptor.

In conclusion, a number of changes occurred in the interaction of K65A P2X3 with a range of nucleotide agonists, compared with results obtained with wt P2X3. These results were difficult to evaluate systematically by calculating the three aforementioned parameters for the concentration-response curves. It should be noted that, when the recovery from desensitization was also measured, an even more complex picture emerged. I_{max} values could not be reliably determined in many cases, because practical considerations limited the use of extremely high concentrations of agonists. Therefore, we decided to simulate the original current tracings according to the hidden Markov model (Fig. 2C). The rate constants characterizing transitions between the unbound, closed-state receptor (C_1), and the receptor binding one (C_2), two (C_3), or three (C_4) agonist molecules, as well the two open-state receptors (O_1 and O_2) and the desensitized receptors (D_1, D_2, D_3, and D_4), are indicated. By changing the on- and off-rate constants k_1/k_{-1} or l_{-1} and d_1/d_{-1}, the shape and amplitude of the agonist-induced currents could be computer-modeled. All calculated rate constants are presented (Supplemental Table 1). The rather good quality of the fits can be judged from the parallelism of the original current recordings and the calculated current traces. Fits for the agonist currents were computed by modifying the rate constants for each agonist (e.g., currents at the wt P2X3 receptor) (Fig. 3) and each receptor mutant (e.g., currents at the mutant receptors with ATP as an agonist) (Fig. 4). In the case of nonoptimal fits, it should be noted that we overlaid the mean fits from all experiments in a group on a tracing recorded from an individual cell in this group of experiments.

In Figs. 3 and 4, we show the effects of increasing agonist concentrations and the measurement of recovery rates. It is noteworthy that large differences in the amplitudes of current responses existed (e.g., comparison of the effect of 1000 μM ATP at K176A and that of 100 μM ATP at wt P2X3) (Fig. 4). The range of agonist concentrations varied between 0.01 and 3 μM for ATP and between 3 and 1000 μM for GTP at the wt receptor (Fig. 3), between 0.3 and 100 μM for ATP at F174A, and between 3 and 1000 μM ATP at K65A (Fig. 4). The rates of desensitization and recovery from desensitization showed great variability (N279A and R281A desensitized slowly and their recovery rates were fast) (Fig. 4). The desensitization at K176A was almost nonexistent, but this mutant also responded to ATP with almost negligible current amplitudes. Instead of the use of parameters to describe these individual phenomena, binding energies were calculated as a universal characteristic of a certain agonist and a certain receptor mutant.

As additional proof of the quality of our computer simulation, concentration-response curves were constructed for each fitted agonist-induced current at the wt P2X3 receptor and its K65A mutant, and curves were compared with the corresponding experimentally measured data (Table 1 and Supplemental Fig. 1). On the basis of the rate constants derived from the current measurements, the binding energy for a certain agonist with a given mutant was calculated. These values were compared with the binding energies calculated from measurements with the same agonist with the wt receptor and ATP with the mutant receptor (Fig. 5A). The energy difference in the case of an independent influence of a change in agonist structure on the one hand and receptor structure on the other is 0; we allowed a random range of <5 kJ/mol for the threshold level of $\Delta\Delta G$, above which a significant direct interaction between the agonist and the mutated AA was assumed (Fig. 5B).

The binding energies for all investigated mutants are shown in Fig. 5. ATP itself exhibited a binding energy of -35.7 ± 0.01 kJ/mol ($n = 14$) at the wt P2X3 receptor (Fig. 5A). This binding energy was decreased with all Ala mutants investigated but to the greatest degree with K176A, N279A, and R281A. Changes with respect to ATP occurred at Lys65 (β,γ-me-ATP, dATP, and 2-MeS-ATP), Lys176 (α,β-me-ATP), Arg281 (ATP-γ-S), and Phe301 (ATP-γ-S) (Fig. 5B). We suggest that these AA residues are of particular importance for the binding of ATP and its analogs. The replacement of the nonconserved aromatic amino acid Phe174 by Ala failed to alter the current responses to all investigated agonists, compared with results obtained with the wt receptor (Fig. 5). K176A was the only investigated mutant with which the P2X1/3-selective agonist α,β-me-ATP exhibited a marked decrease in binding energy, in comparison with ATP itself (Fig. 5B). Although α,β-me-ATP at up to 3 mM did not activate the receptor, the other agonists remained effective. It is noteworthy that desensitization to ATP also markedly decreased with this mutant (Fig. 4). In contrast to the wt receptor, with which 2-MeS-ATP had the highest affinity, 2-MeS-ATP and ATP exhibited comparable binding energies with N279A (Fig. 5A), which resulted in a decrease in the relative binding energy (Fig. 5B).

With the R281A mutant, which was a direct neighbor of Asn279 in a β-sheet structure, we observed decreased receptor desensitization to ATP (Fig. 4). This effect was most prominent for α,β-me-ATP and ATPγS (data not shown). Moreover, binding of ATPγS to the wt receptor was weaker than that of ATP (Fig. 5A). Replacement of Arg by Ala at position 281 turned this relationship into its opposite (Fig. 5B), which possibly indicates that the γ-phosphate of ATP interacts with the side chain of Arg281. In contrast, the replacement of Leu with Ala at position 297 had no major effect. It is interesting to note that the mutation of Arg281 to Ala caused selective improvement in the binding of ATP-γ-S and the mutation of Phe301 by Ala acted in a similar manner.

The applicability to receptor-ligand interactions of the double-mutant cycle method, which was originally developed for AA interactions, was checked with additional measurements of current responses to ATP, α,β-me-ATP, ATP-γ-S, and GTP with the H45A mutant. This AA is located in the extracellular loop near transmembrane region 1, outside the binding site. The binding energies in these control experiments with H45A remained below the arbitrary energy threshold level of

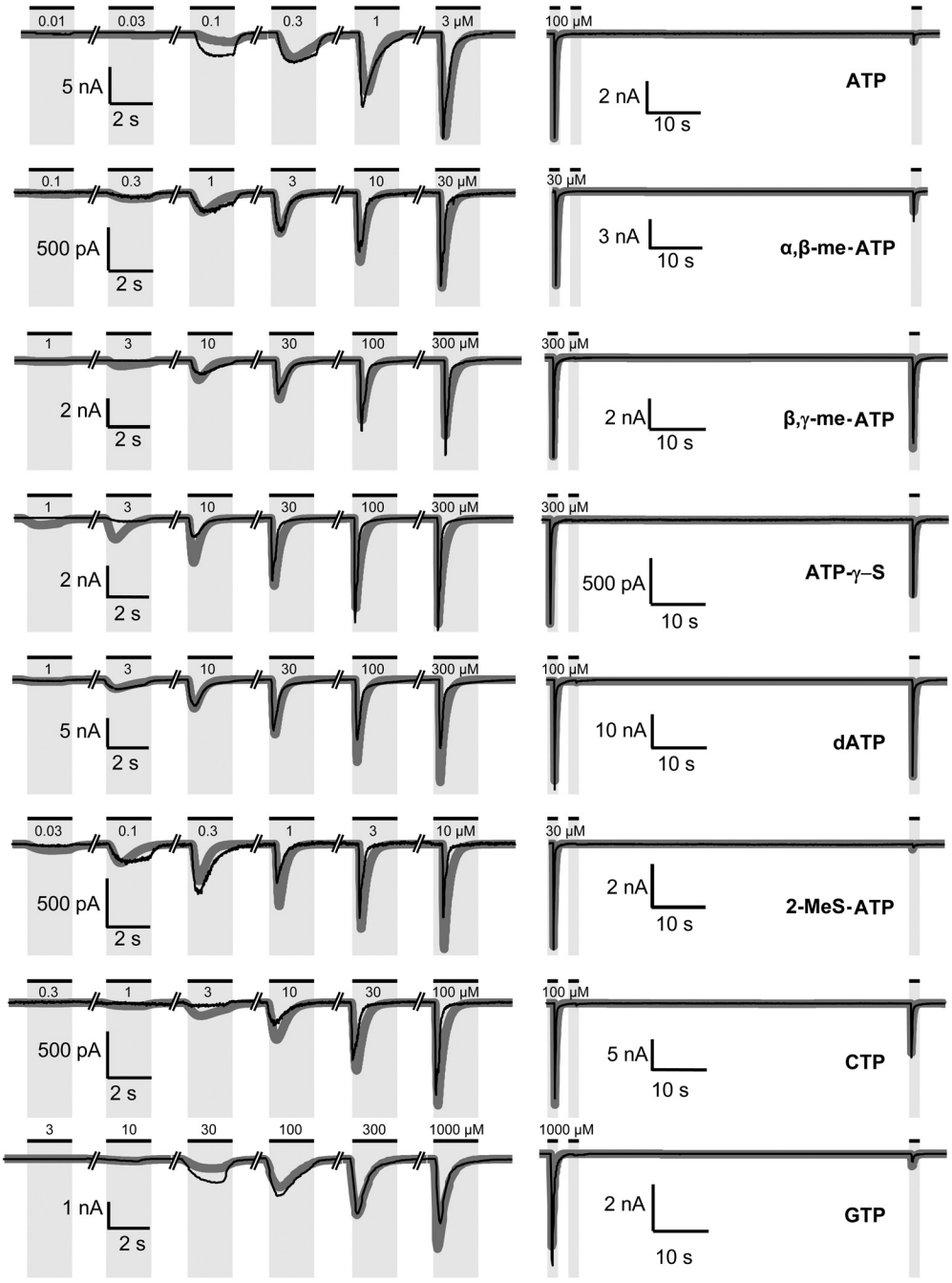

Fig. 3. Measured and simulated currents induced by ATP, its structural analogs, and CTP at wt P2X3 receptors expressed in HEK293 cells. Increasing agonist concentrations were applied locally for 2 s every 5 min (left). Recovery protocols were produced by applying a high agonist concentration for 2 s, again after a 2-s interval, and finally after an additional 60-s interval (right). Thin black lines, representative current traces of four to 16 similar experiments. Thick gray lines, current traces calculated with a hidden Markov model based on kinetic fits. Horizontal lines, agonist application times.

5 kJ/mol, which was set to represent a meaningful difference from 0 ($\Delta\Delta G$: α,β-me-ATP, 1.77 ± 0.03 kJ/mol; ATP-γ-S, −1.47 ± 0.02 kJ/mol; GTP, −1.47 ± 0.05 kJ/mol).

Agonists used in this study were docked to the binding pouch of the P2X3 receptor, as described in *Materials and Methods*. In addition to the relatively small ligands tested, Bz-ATP and trinitrophenyl-ATP (TNP-ATP) were docked to determine whether the binding configuration was applicable to these larger molecules (Fig. 6). The docking poses with the smallest R.M.S.D. values between ATP and the other ligands were chosen as being the most likely ones. The modeled configuration is in agreement with our experimental results and provides enough space for molecules with bulky side chains, such as Bz-ATP and TNP-ATP. The position of the benzoyl groups of Bz-ATP can reach residues at the head domain of the "dolphin," which are known to increase the effect of ATP at rat P2X7 (Young et al., 2007). In our favored binding configuration, the adenine ring is located close to this residue, which makes it possible that the thiol group in 8-thiocyano-ATP binds to the cysteine residue engineered into Leu186 of rat P2X2 through a proximity-dependent tethering reaction (Phe174 with P2X3 numbering) (Jiang et al., 2011).

Discussion

On the basis of mutagenesis studies, four different molecular models for the agonist binding site were proposed, none of which was consistent with the binding site constructed from the published crystal structure of the zfP2X4 receptor (Kawate et al., 2009; Browne et al., 2010; Young, 2010). First,

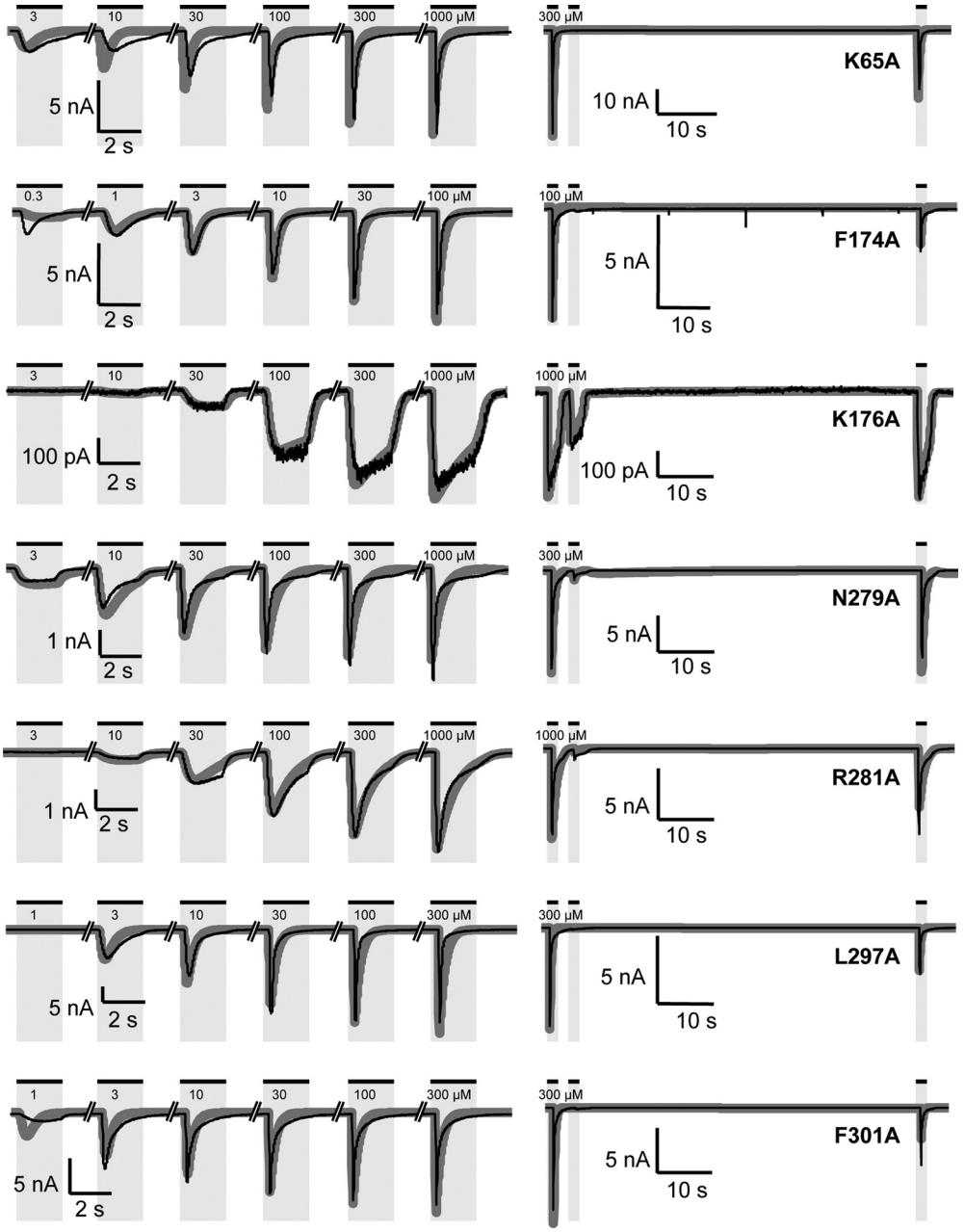

Fig. 4. Measured and simulated currents induced by ATP at P2X3 binding site mutants expressed in HEK293 cells. Increasing ATP concentrations were applied locally for 2 s every 5 min (left). Recovery protocols were produced by applying a high ATP concentration for 2 s, then again after a 2-s interval, and finally after an additional 60-s interval (right). Thin black lines, representative current traces of four to eight similar experiments. Thick gray lines, current traces calculated with a hidden Markov model based on kinetic fits. Horizontal lines, agonist application times.

it was suggested that the ATP action is coordinated by positively charged lysine residues interacting with the negatively charged phosphate tail of ATP and the adenine ring is coordinated by the aromatic phenylalanine residues Phe185 and Phe291 in P2X1 (Phe171 and Phe280 with P2X3 numbering) (Roberts et al., 2006; Evans, 2010). However, Phe174 is located outside the binding pouch and ~10 Å away from our favored binding configuration. Phe280 is located between Asn279 and Arg281 but at the opposing side of the β-strand, which is buried in the crystal structure. A slight conformational change of the receptor after ATP binding may move the adenine ring nearer to Phe280, helping to establish π-stacking. The suggestion that the lysine residues interact with the phosphate tail of ATP is certainly valid, although with some limitations. The replacement of Lys63 by Ala, for example, abolished the effect of α,β-me-ATP (Bodnar et al., 2011) but Lys63 is positioned at a site relatively far from other AAs (Arg281 and Arg295) that coordinate phosphate binding, which makes a direct interaction unlikely (Fig. 6). Second, an alternative scenario was proposed on the basis of the similarity of the second half of the extracellular domain of P2X4 receptors with the catalytic domain of class II aminoacryltRNA synthetase (Freist et al., 1998; Yan et al., 2005). Third, a model was constructed by performing a secondary structure alignment of P2X2 receptors with ASIC channels as a template (Guerlet et al., 2008). None of the latter models shared major similarities with the zfP2X4 structure; we know, for example, that P2X and ASIC possess very different secondary structures and folds, although they do share striking similarities of their transmembrane domains and pore architecture (Gonzales et al., 2009; Young, 2010).

Fourth, our own previous model of P2X3 was constructed by using a combination of secondary structure prediction and mutagenesis data, and it suggested the existence of four

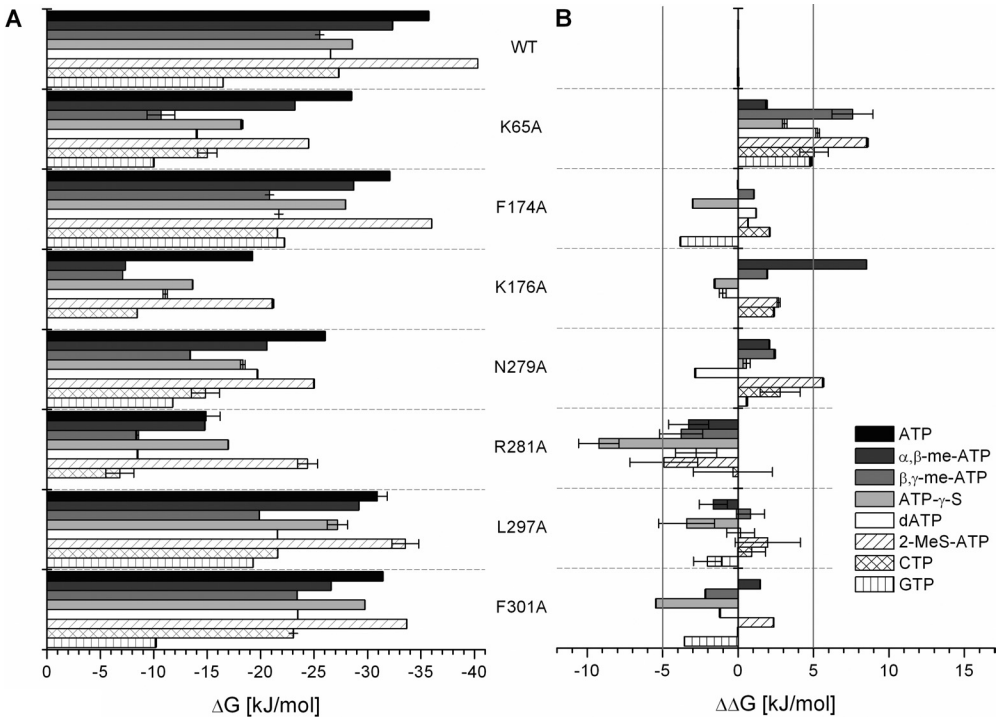

Fig. 5. Binding energies of ATP, its structural analogs, and CTP at wt P2X3 receptors and their binding site mutants. A, absolute binding energies (ΔG) calculated from k_1 and k_{-1} from the kinetic fits. B, differences between the predicted and measured binding energies ($\Delta\Delta G$). Positive values represent measured binding energies of agonist mutant pairings that are lower and negative values represent binding energies than are higher than the predicted ones (all of these results differed in a statistically significant manner from 0; $P < 0.05$). Energy differences over a randomly set threshold level of 5 kJ/mol (gray lines) were interpreted as indicating noticeable interaction between the agonist and the receptor containing the mutated amino acid. Each column indicates the means calculated from four to 13 experiments. Error bars were derived from the propagated S.D. values for k_1 and k_{-1} in the kinetic fits.

putative NBSs within a single subunit (Mager et al., 2004; Fischer et al., 2007). These NBSs, located pairwise at two neighboring subunits, were shown to form the agonist binding pouch (Bodnar et al., 2011). We replaced systematically all conserved AAs and a few nonconserved AAs with Ala and found in some cases complete blockade of membrane currents in response to the application of α,β-me-ATP to P2X3 receptors expressed in HEK293 cells. Other AAs seemed to be less important for the agonist effect, although Ala replacement decreased receptor function.

In the present study, we selected mutant P2X3 receptors that still responded to α,β-me-ATP, although with lower intensity than wt receptors, and we tested a range of ATP structural analogs in addition to ATP itself. The pyrimidine nucleotide CTP was also used, because it is known to be a slowly desensitizing, weak agonist at P2X3 receptors (Chen et al., 1995). Two complementary methodological approaches were used. On the basis of a kinetic fit of the P2X3 receptor current with a hidden Markov model, the binding energies of each agonist were calculated for both the wt receptor and selected mutants. With this information, it was possible to decide whether the effect of a certain agonist was particularly sensitive to a given mutation. A homology model of the P2X3 agonist binding pouch was constructed on the basis of the crystal structure of zfP2X4. ATP and its structural analogs were docked to the binding pocket to compare the functional data with the structural data.

Two pieces of information may be of interest for the understanding of the present computer simulation data. The kinetic model used by us was based on a refinement of the original cyclic model for P2X3 operation described by Sokolova et al. (2006). We added an additional step to the model, assuming that both diligand and triliganded receptors could open upon agonist exposure (Karoly et al., 2008). This correction resulted in better fits of the P2X3 current traces. Moreover, saturation binding experiments performed with the high-affinity purinergic agonist [^{3}H]α,β-me-ATP and P2X3-HEK293 cells allowed determination of the binding energy ΔG with a biochemical method (Varani et al., 2008). The binding energy measured at 20°C was approximately −47 kJ/mol, which correlated reasonably well with the present ΔG value (approximately −36 kJ/mol) determined electrophysiologically at 20 to 22°C.

Inspection of Fig. 5B and comparison of the data shown therein with those derived from the docking experiments shown in Fig. 6 allow the following main conclusions. First, Lys65 seems to be a central amino acid that may coordinate the binding of the purine, the ribose moiety, and the phosphate chain of ATP. The replacement of Lys by Ala at position 65 interfered strongly with the binding of 2-MeS-ATP, dATP, and β,γ-me-ATP, in comparison with the binding of ATP itself. Second, the Phe174 side chain is located behind the side chain of Lys63, with complete loss of function when Lys63 is replaced by Ala. Indirect changes to provide more space for positioning agonists in the P2X3 binding groove through replacement of Phe174 by the smaller Ala were, despite our expectations, without effect. Third, the currents induced by any of the agonists were greatly depressed but not abolished with the K176A P2X3 receptor. In contrast, there was no current response to α,β-me-ATP. This finding cannot be explained by our homology model because Lys176 is located relatively far away from the binding pouch in the closed state, although this situation might be altered when the receptor transits into the open state. Fourth, the selective deterioration of the 2-MeS-ATP effect at the N279A mutant can be explained by the close proximity of this Asn residue to the methylthio group attached to the pyrimidine ring of ATP. Fifth, Arg281 is also located near the γ-phophate of ATP, which explains the selective, although in this case positive, modulation of the ATP-γ-S effect. Sixth, Phe301 is not expected to alter directly the docking of ATP-γ-S to the receptor, despite its increased binding energy in comparison with ATP. However, an

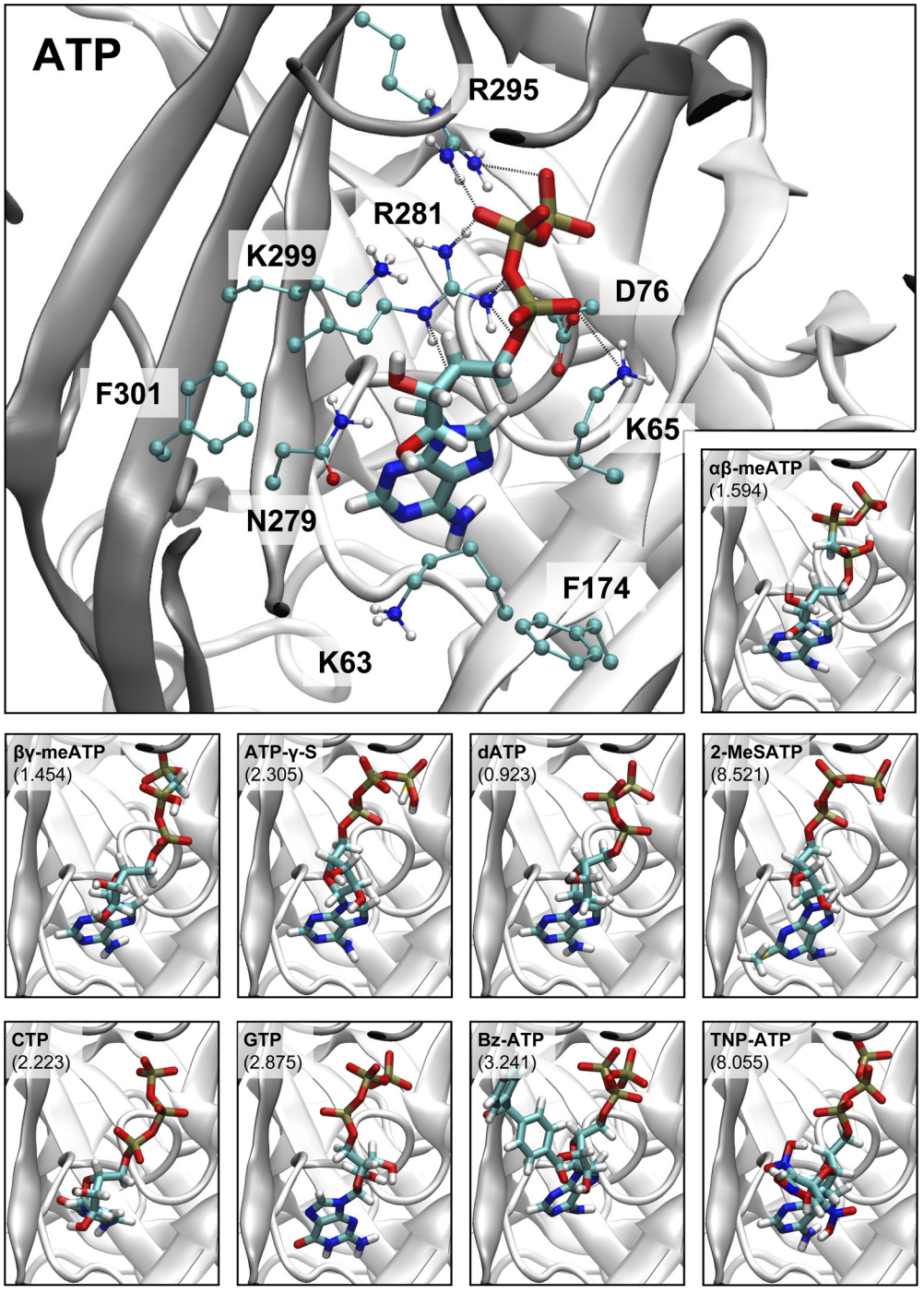

Fig. 6. Homology model of the P2X3 receptor with docked ATP^{4-}. AAs involved in agonist binding are situated at the interface of two neighboring subunits (shown in gray and white). The side chains of relevant AAs forming the binding pouch are shown as balls and sticks and are labeled with their one-letter codes. Distances between the nitrogen and oxygen atoms of the AAs and ATP of less than 3.2 Å are indicated by dashed lines. Color coding was as follows: carbon, cyan; oxygen, red; nitrogen, blue; phosphorus, gold; hydrogen, white; sulfur, yellow. Asp76, positioned at the posterior wall of the binding pouch, is also indicated. The R.M.S.D. values for the positioning of the nucleotide analogs are shown in the left upper corner and were calculated in relation to ATP.

indirect interaction with the docking of the γ-phosphate moiety may occur through an effect at the nearby Arg281. Seventh, all conclusions are valid only for a number of conserved and nonconserved AAs that were selected on the basis of their maintained response to α,β-me-ATP and their orientations toward the groove of the binding pouch.

Our experiments suggest that an electrostatic attraction between basic AAs and the negatively charged phosphate chain may occur as a long-range interaction, which is realized during the first contact between the receptor protein and its ligand. It is somewhat surprising that, despite the original assumption (Roberts et al., 2006), the prerequisites for such an interaction existed between Arg rather than Lys molecules on the one hand and ATP or its analogs on the other. The double-mutant cycle approach requires measurable binding energies, which are not given for K63A and K299A. For this reason, these AAs had to be excluded from our study. However, ATP docking to the receptor suggested involvement in ligand binding for both AAs.

In conclusion, we measured the binding energies for a range of nucleotide agonists with wt or mutant P2X3 receptors in a double-mutant cycle paradigm, and we constructed a homology model of human P2X3 on the basis of the crystal structure of zfP2X4. Data obtained with the two approaches were fully consistent and yielded a receptor model that might be helpful for future structure-activity relationship studies.

Authorship Contributions

Participated in research design: Riedel and Illes.

Conducted experiments: Wiese and Leichsenring.

Performed data analysis: Riedel, Wiese, and Illes.

Wrote or contributed to the writing of the manuscript: Riedel and Illes.

References

Aschrafi A, Sadtler S, Niculescu C, Rettinger J, and Schmalzing G (2004) Trimeric architecture of homomeric P2X2 and heteromeric P2X1+2 receptor subtypes. *J Mol Biol* **342:**333–343.

Bean BP (1990) ATP-activated channels in rat and bullfrog sensory neurons: concentration dependence and kinetics. *J Neurosci* **10:**1–10.

Bodnar M, Wang H, Riedel T, Hintze S, Kato E, Fallah G, Gröger-Arndt H, Giniatullin R, Grohmann M, Hausmann R, et al. (2011) Amino acid residues constituting the agonist binding site of the human P2X3 receptor. *J Biol Chem* **286:**2739–2749.

Browne LE, Jiang LH, and North RA (2010) New structure enlivens interest in P2X receptors. *Trends Pharmacol Sci* **31:**229–237.

Chen CC, Akopian AN, Sivilotti L, Colquhoun D, Burnstock G, and Wood JN (1995) A P2X purinoceptor expressed by a subset of sensory neurons. *Nature* **377:**428–431.

Ding S and Sachs F (1999) Single channel properties of P2X2 purinoceptors. *J Gen Physiol* **113:**695–720.

Egan TM, Cox JA, and Voigt MM (2004) Molecular structure of P2X receptors. *Curr Top Med Chem* **4:**821–829.

Evans RJ (1996) Single channel properties of ATP-gated cation channels (P2X receptors) heterologously expressed in Chinese hamster ovary cells. *Neurosci Lett* **212:**212–214.

Evans RJ (2010) Structural interpretation of P2X receptor mutagenesis studies on drug action. *Br J Pharmacol* **161:**961–971.

Fischer W, Zadori Z, Kullnick Y, Gröger-Arndt H, Franke H, Wirkner K, Illes P, and Mager PP (2007) Conserved lysin and arginin residues in the extracellular loop of P2X(3) receptors are involved in agonist binding. *Eur J Pharmacol* **576:**7–17.

Fiser A and Sali A (2003) Modeller: generation and refinement of homology-based protein structure models. *Methods Enzymol* **374:**461–491.

Freist W, Verhey JF, Stühmer W, and Gauss DH (1998) ATP binding site of P2X channel proteins: structural similarities with class II aminoacyl-tRNA synthetases. *FEBS Lett* **434:**61–65.

Gerevich Z, Zadori ZS, Köles L, Kopp L, Milius D, Wirkner K, Gyires K, and Illes P (2007) Dual effect of acid pH on purinergic P2X3 receptors depends on the histidine 206 residue. *J Biol Chem* **282:**33949–33957.

Gonzales EB, Kawate T, and Gouaux E (2009) Pore architecture and ion sites in acid-sensing ion channels and P2X receptors. *Nature* **460:**599–604.

Grote A, Boldogkoi Z, Zimmer A, Steinhäuser C, and Jabs R (2005) Functional characterization of P2X3 receptors fused with fluorescent proteins. *Mol Membr Biol* **22:**497–506.

Guerlet G, Taly A, Prado de Carvalho L, Martz A, Jiang R, Specht A, Le Novère N, and Grutter T (2008) Comparative models of P2X2 receptor support inter-subunit ATP-binding sites. *Biochem Biophys Res Commun* **375:**405–409.

Horovitz A (1996) Double-mutant cycles: a powerful tool for analyzing protein structure and function. *Fold Des* **1:**R121–R126.

Humphrey W, Dalke A, and Schulten K (1996) VMD: visual molecular dynamics. *J Mol Graph* **14:**33–38.

Jiang LH, Rassendren F, Surprenant A, and North RA (2000) Identification of amino acid residues contributing to the ATP-binding site of a purinergic P2X receptor. *J Biol Chem* **275:**34190–34196.

Jiang R, Lemoine D, Martz A, Taly A, Gonin S, Prado de Carvalho L, Specht A, and Grutter T (2011) Agonist trapped in ATP-binding sites of the P2X2 receptor. *Proc Natl Acad Sci USA* **108:**9066–9071.

Karoly R, Mike A, Illes P, and Gerevich Z (2008) The unusual state-dependent affinity of P2X3 receptors can be explained by an allosteric two-open-state model. *Mol Pharmacol* **73:**224–234.

Kawate T, Michel JC, Birdsong WT, and Gouaux E (2009) Crystal structure of the ATP-gated P2X(4) ion channel in the closed state. *Nature* **460:**592–598.

Khakh BS, Burnstock G, Kennedy C, King BF, North RA, Séguéla P, Voigt M, and Humphrey PP (2001) International Union of Pharmacology. XXIV. Current status of the nomenclature and properties of P2X receptors and their subunits. *Pharmacol Rev* **53:**107–118.

Köles L, Fürst S, and Illes P (2007) Purine ionotropic (P2X) receptors. *Curr Pharm Des* **13:**2368–2384.

Mager PP, Weber A, and Illes P (2004) Bridging the gap between structural bioinformatics and receptor research: the membrane-embedded, ligand-gated, P2X glycoprotein receptor. *Curr Top Med Chem* **4:**1657–1705.

Marquez-Klaka B, Rettinger J, and Nicke A (2009) Inter-subunit disulfide cross-linking in homomeric and heteromeric P2X receptors. *Eur Biophys J* **38:**329–338.

Milescu LS, Akk G, and Sachs F (2005) Maximum likelihood estimation of ion channel kinetics from macroscopic currents. *Biophys J* **88:**2494–2515.

Nicke A, Bäumert HG, Rettinger J, Eichele A, Lambrecht G, Mutschler E, and Schmalzing G (1998) P2X1 and P2X3 receptors form stable trimers: a novel structural motif of ligand-gated ion channels. *EMBO J* **17:**3016–3028.

North RA (2002) Molecular physiology of P2X receptors. *Physiol Rev* **82:**1013–1067.

Roberts JA and Evans RJ (2007) Cysteine substitution mutants give structural insight and identify ATP binding and activation sites at P2X receptors. *J Neurosci* **27:**4072–4082.

Roberts JA, Vial C, Digby HR, Agboh KC, Wen H, Atterbury-Thomas A, and Evans RJ (2006) Molecular properties of P2X receptors. *Pflugers Arch* **452:**486–500.

Shinozaki Y, Sumitomo K, Tsuda M, Koizumi S, Inoue K, and Torimitsu K (2009) Direct observation of ATP-induced conformational changes in single P2X4 receptors. *PLoS Biol* **7:**e103.

Sokolova E, Skorinkin A, Fabbretti E, Masten L, Nistri A, and Giniatullin R (2004) Agonist-dependence of recovery from desensitization of P2X(3) receptors provides a novel and sensitive approach for their rapid up or downregulation. *Br J Pharmacol* **141:**1048–1058.

Sokolova E, Skorinkin A, Moiseev I, Agrachev A, Nistri A, and Giniatullin R (2006) Experimental and modeling studies of desensitization of P2X3 receptors. *Mol Pharmacol* **70:**373–382.

Trott O and Olson AJ (2010) AutoDock Vina: improving the speed and accuracy of docking with a new scoring function, efficient optimization, and multithreading. *J Comput Chem* **31:**455–461.

Varani K, Surprenant A, Vincenzi F, Tosi A, Gessi S, Merighi S, and Borea PA (2008) Binding thermodynamic characterization of human P2X1 and P2X3 purinergic receptors. *Biochem Pharmacol* **75:**1198–1208.

Vial C, Roberts JA, and Evans RJ (2004) Molecular properties of ATP-gated P2X receptor ion channels. *Trends Pharmacol Sci* **25:**487–493.

Wilkinson WJ, Jiang LH, Surprenant A, and North RA (2006) Role of ectodomain lysines in the subunits of the heteromeric P2X2/3 receptor. *Mol Pharmacol* **70:**1159–1163.

Yan Z, Liang Z, Tomic M, Obsil T, and Stojilkovic SS (2005) Molecular determinants of the agonist binding domain of a P2X receptor channel. *Mol Pharmacol* **67:**1078–1088.

Young MT (2010) P2X receptors: dawn of the post-structure era. *Trends Biochem Sci* **35:**83–90.

Young MT, Fisher JA, Fountain SJ, Ford RC, North RA, and Khakh BS (2008) Molecular shape, architecture, and size of P2X4 receptors determined using fluorescence resonance energy transfer and electron microscopy. *J Biol Chem* **283:**26241–26251.

Young MT, Pelegrin P, and Surprenant A (2007) Amino acid residues in the P2X7 receptor that mediate differential sensitivity to ATP and BzATP. *Mol Pharmacol* **71:**92–100.

Zemkova H, Yan Z, Liang Z, Jelinkova I, Tomic M, and Stojilkovic SS (2007) Role of aromatic and charged ectodomain residues in the P2X(4) receptor functions. *J Neurochem* **102:**1139–1150.

Address correspondence to: Dr. Thomas Riedel, Rudolf Boehm Institute for Pharmacology and Toxicology, University of Leipzig, Haertelstrasse 16-18, 04107 Leipzig, Germany. E-mail: thomas.riedel@medizin.uni-leipzig.de